Numerical Modeling of the Material Deposition and Contouring Precision in Fused Deposition Modeling

Comminal, R.; Serdeczny, M. P.; Pedersen, D. B.; Spangenberg, J.

Published in:
Proceedings of the Annual International Solid Freeform Fabrication Symposium

Publication date:
2018

Document Version
Publisher's PDF, also known as Version of record

Solid Freeform Fabrication 2018: Proceedings of the 29th Annual International Solid Freeform Fabrication Symposium – An Additive Manufacturing Conference
Reviewed Paper

NUMERICAL MODELING OF THE MATERIAL DEPOSITION AND CONTOURING PRECISION IN FUSED DEPOSITION MODELING

R. Comminal, M. P. Serdeczny, D. B. Pedersen, and J. Spangenberg

Department of Mechanical Engineering, Technical University of Denmark, Kgs. Lyngby, Denmark

Abstract

We present a numerical model of the material deposition in fused deposition modeling. The flow of the material extruded from the printing head nozzle is simulated within the computation fluid dynamics (CFD) paradigm. The molten thermoplastic is modeled as an incompressible Newtonian fluid with a free surface. The numerical model provides a prediction of the shape of the printed road. Four deposition strategies are investigated to print a road along a tool path with a 90° turn. The investigated scenarios include the ideal case of an extrusion rate synchronized with the printing speed, as well as the cases of a sharp tool path with a stop-at-turn trajectory, and a smoothed tool path with blended acceleration. The CFD simulation provides a way to optimize the tool path planning and the deposition strategy, in order to improve dimensional accuracy in extrusion-based additive manufacturing.

Introduction

Fused deposition modeling (FDM) is an extrusion-based additive manufacturing process, where a semi-molten thermoplastic is extruded and deposited along a prescribed road, onto a build platform. The extruded thermoplastic bonds to neighboring materials as it solidifies, thereby creating a 3D-printed component. The printing head consists of a liquefier that melts the thermoplastic and a nozzle that extrudes it. The feedstock material is supplied to the printing head as a filament driven by pinch rollers. The pressure inside the extrusion nozzle is provided by the torque of the drive pinch rollers that forces the filament through the printing head [1]. The printing head and the build platform are mounted on a three-axis gantry that controls the relative position of the printing head in the reference frame of the build platform.

Prior fabrication, the CAD model of the part is analyzed by a slicer software that generates the G-code containing all the machine instructions for the fabrication. The G-code decomposes the entire tool path into segments and curves and specifies the amount of material to be extruded along each section. The material is deposited layer by layer, and each layer is generally printed in two operations. First, the boundary of the layer is deposited, via a contouring pattern consisting in one or more roads. Then, the interior of the layer is printed, using a prescribed filling pattern. Slicer software provides a variety of filling patterns, both for dense and hollow parts. The choice of the filling pattern has a high impact on the mechanical properties and the build time of the part [2]. Other parameters specified to the slicer, such as the layer height, the infill density, the printing speed, and the extrusion multiplier also have a significant influence on the dimensional accuracy and the surface quality [3, 4, 5, 6]. Afterwards, the G-code is read by the firmware of the 3D-printer, e.g. Marlin software [7], which translates the instructions of the G-code into numerical commands to the actuators of the 3D printer. The firmware calculates appropriate acceleration profiles, according to the characteristics of the motors (i.e. their maximum acceleration and jerk).

Modern firmware may also smooth the sharp corners of the tool paths, in order to negotiate turns with blended acceleration, instead of stopping the printing head at the turn points. Moreover, open source firmware can be tuned by advanced users to improve printing performances.

The printing resolution of the FDM process depends on the prescribed tool path, the positioning precision of the gantry, the layer thickness and the road width. Whereas current desktop 3D-printer are usually operated via open loop controls, Weiss et al. [8] have shown that close loop controls can significantly reduce the positioning errors and improve the acceleration performance of the gantry. The road width depends on the ratio t/D of the layer thickness (user-specified parameter) by the nozzle diameter (machine specific parameter), as well as the ratio V_p/V_e of the printing speed (i.e. the velocity of the printing head) by the extrusion rate (i.e. the extrusion volumetric flux) [9]. As the ratio t/D is fixed during the process, a uniform road width requires a constant velocity ratio V_p/V_e. In practice however, the extrusion rate is not adjusted, while the printing speed varies along curved tool paths and turns, as the printing head needs to deceleration and acceleration to change direction [10]. The main reasons for keeping a constant extrusion rate are the lack of feedback control and the time delay between the acceleration of the drive rollers and the variations of extrusion rate, caused by the non-linearity of the liquefier-extruder system. Hence, the decrease of the printing head speed near turns generates material overfills. Moreover, the smoothing of the tool path at the corner may result in additional overfills and underfills [11]. Han et al. [11] proposed a tool path-based deposition planning, where segments of similar lengths are grouped together and each group is assigned an extrusion rates depending on the average segment length. This algorithm was shown to reduce overfill and underfill in dense filling pattern [12]. Real-time regulation of the filament feed rate as a function of the printing head speed were proposed in [13, 14, 15]. However, the actual implementation of a real-time controller requires a reliable model of the dynamical response of the liquefier-extruder system. In addition, Ertay et al. [15] proposed an adaptive control of the heating system as a function of the extrusion rate, and a smoothing of the tool path. Their method demonstrated a reduction of overfills along smoothed curved tool paths. Marlin firmware also provides the possibility to regulate the angular velocity of the drive rollers as a function of the printing speed. This option, termed *Linear Advance*, takes into account the time delay in the variations of the extrusion rate caused by material compressibility as the liquefier undergoes pressure changes. Nevertheless, the Linear Advance option requires a calibration of the 3D printer for the material being printed.

A physics-based dynamical model of the liquefier-extruder system was derived by Bellini et al. [16], who proposed a transfer function relating the extrusion rate to the torque of the drive rollers. Their model showed that the temperature-dependency of the melt viscosity and the limitation of torque and power of the drive rollers' motors can be responsible for the time delay in the extrusion rate response, while steady-state errors can be caused by the slippage between filament and rollers. Jiang and Gu [17] suggested a mechanisms of extrusion rate instabilities, occurring when the required torque of the drive rollers exceeds the maximum capacity of the motor (during acceleration phases). Moreover, an empirical relationship between the maximum achievable extrusion rate (before failure) and the extrusion temperature was found by Mackay et al. [18].

Computation fluid dynamics (CFD) models have been used in [9, 19, 20, 21] to simulate the material deposition in FDM. Comminal et al. [9] showed that the shape of deposited road depends on the normalized layer thickness t/D and the normalized printing speed V_p/V_e. Du et al. [19] investigated the effect of laser-assisted heating on the morphology of the deposited road. Xia

et al. [20, 21] developed a thermo-fluid model which focuses on the cooling stage and the solidification of the molten material, after the deposition.

In this paper, we use a CFD model to simulate the material deposition along a road with a 90° turn. The numerical simulation predicts the variations of the road width along the tool path and enables a visualization of overfill and underfill regions at the turn. Different depositions strategies are simulated, in order to investigate the effects of smoothing the tool path and having a constant versus a synchronized extrusion rate.

Deposition strategy at 90° turns

Four deposition strategies have been investigated for printing a road with a 90° turn, onto the build platform. We assume that the two segments forming the 90° turn are parallel to the X and Y axis of the build platform. With this assumption, the deceleration/acceleration of the printing head at the end/start of the segment are independent from each other. In our numerical model, the motion of the printing head along the two directions of the build platform is governed by three parameters: the cruising speed, the jerk and the maximum acceleration. The cruising speed is the maximum value that the velocity components of the tool path will try reach, whenever possible. The jerk corresponds to a velocity jump that occurs instantaneously when the printing head initiates an acceleration or a deceleration phase. Velocity variations above the value of the jerk are achieved via constant acceleration/deceleration equal to the maximum acceleration. Those three parameters are assumed identical for the two axes of the build platform; their values are reported in Table 1.

Table 1: Characteristics of the printing head motion.

Parameter	**Value**
Cruising speed	60 mm/s
Jerk	10 mm/s
Maximum acceleration	1000 mm/s^2

Two types of tool paths are considered for printing the 90° turn, namely the *sharp* and *smoothed* trajectories. The sharp tool path reproduces the exact trajectory of the two segments, which requires a stop of the printing head at the turn point. In contrast, the smoothed tool path negotiates the turn with blended acceleration along the X and Y axis. The acceleration blending factor κ is defined as the ratio of the acceleration time lead τ by the total deceleration time Δt along the X axis:

$$\kappa = \tau / \Delta t$$

where the acceleration time lead is the time interval between the beginning of the acceleration along the Y axis and the end of the deceleration along the X axis, as represented in Figure 1. The velocity profiles and the corresponding printing head trajectories of the sharp tool path ($\kappa = 0$) and two smoothed tool paths ($\kappa = 0.6$ and $\kappa = 1$) are represented in Figure 1. In addition, two extrusion rates are considered: the case of a constant extrusion rate and the case of a synchronized extrusion rate, where the volumetric flux is kept proportional to the tangential velocity of the printing head. The four deposition strategies that we have simulated are summarized in Table 2.

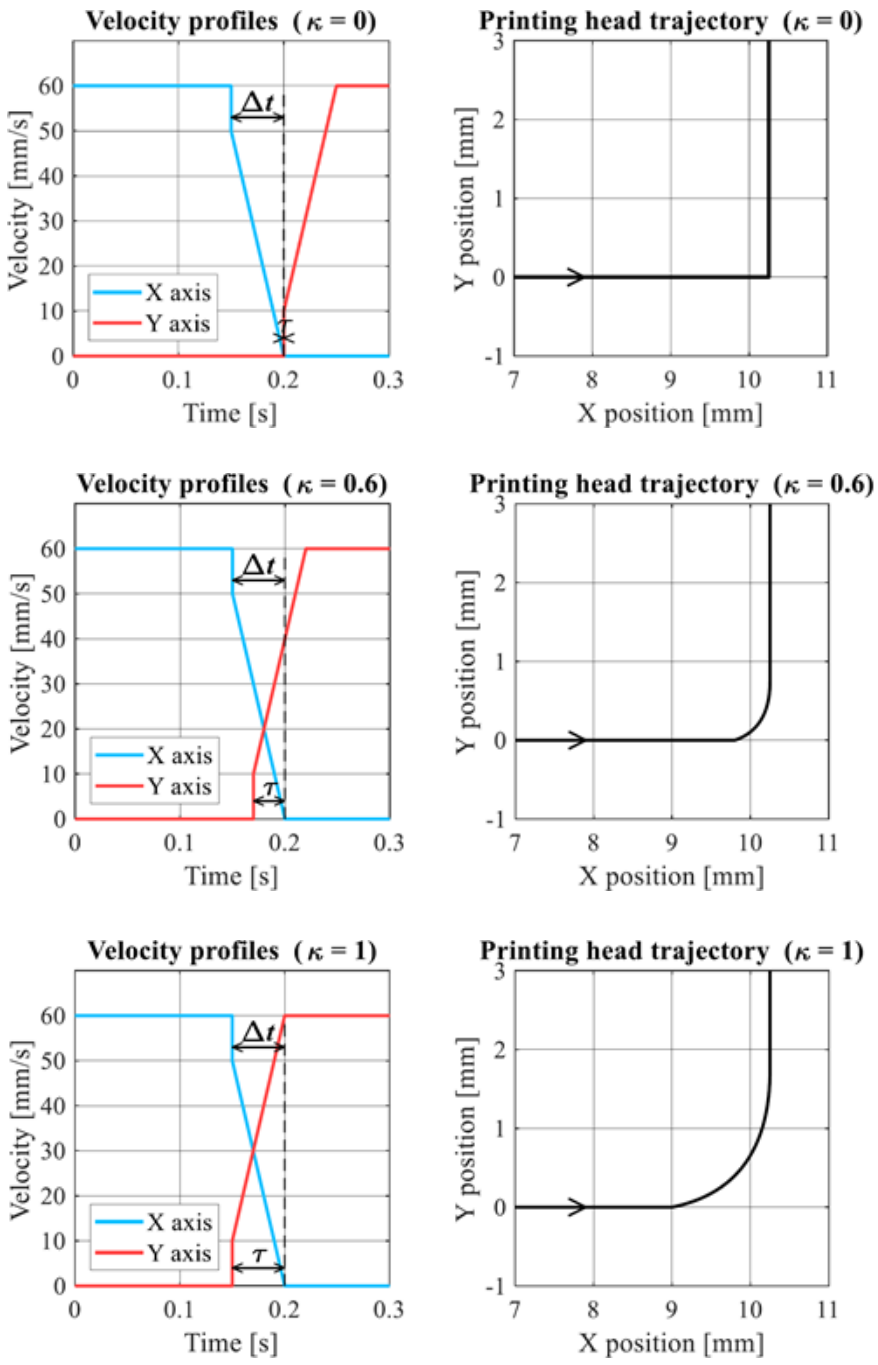

Figure 1: Velocity profiles of the X and Y axis and corresponding printing head trajectories, for different acceleration blending factors κ.

Table 2: Summary of the four deposition strategies simulated.

	Tool path	**Velocity profiles**	**Extrusion rate**
Case 1	Sharp trajectory	Stop at turn $\kappa = 0$	Synchronized
Case 2	Sharp trajectory	Stop at turn $\kappa = 0$	Constant
Case 3	Smoothed trajectory	Blended acceleration $\kappa = 1$	Constant
Case 4	Smoothed trajectory	Blended acceleration $\kappa = 0.6$	Constant

In theory, the synchronized extrusion rate should produce a uniform road width along the turn; however, the synchronized extrusion rate is an ideal case that could only be achieved if the dynamics of the liquefier and the filament feeding system were totally predictable and under full control of the 3D printer, which is not the case in practice. On the other-hand, the constant extrusion rate is expected to lead to variable road widths, when the printing head decelerates or stops at the turn. The next section gives an overview of the numerical model used to simulate the material deposition.

Numerical model

The material deposition was simulated with the commercial software ANSYS® Fluent R18.2 [22]. The geometry of the CFD model consisted in the union of a cylindrical extrusion nozzle and a rectangular volume representing a portion of the build volume, as shown in Figure 2. The dimensions of the rectangular volume were 3.2 × 3.2 × 0.48 mm, while the extrusion nozzle had a diameter 0.4 mm and a conic outer shape with an apex angle of 90 degrees. The layer thickness, defined as the gap between the nozzle orifice and the build platform, was set to 0.32 mm. The position of the printing head was kept fixed during the numerical simulation, while the build platform was moving with prescribed velocities components in the X and Y directions, according to the desired tool path. The extrusion volumetric flux was prescribed at the inlet of the extrusion nozzle, either with a constant value or a value synchronized on the tangential printing velocity.

The computational domain was discretized with a Cartesian cut-cell mesh consisting of 969,090 finite volumes, with a grid spacing of 20 μm in all the directions (there are respectively 160, 160, and 56 elements in the X-, Y- and Z-directions). The velocity and the pressure fields are calculated from the local conservation of mass and momentum inside each finite volume of the mesh. Moreover, the material deposition was modeled as a two-phase flow, where the primary and secondary phases are the molten plastic and the surrounding air. The free-surface of the molten plastic was tracked with the volume-of-fluid method. An implicit coupled pressure-velocity algorithm was selected, to ensure numerical stability. The transient flow was solved with temporal increments of 0.1 ms.

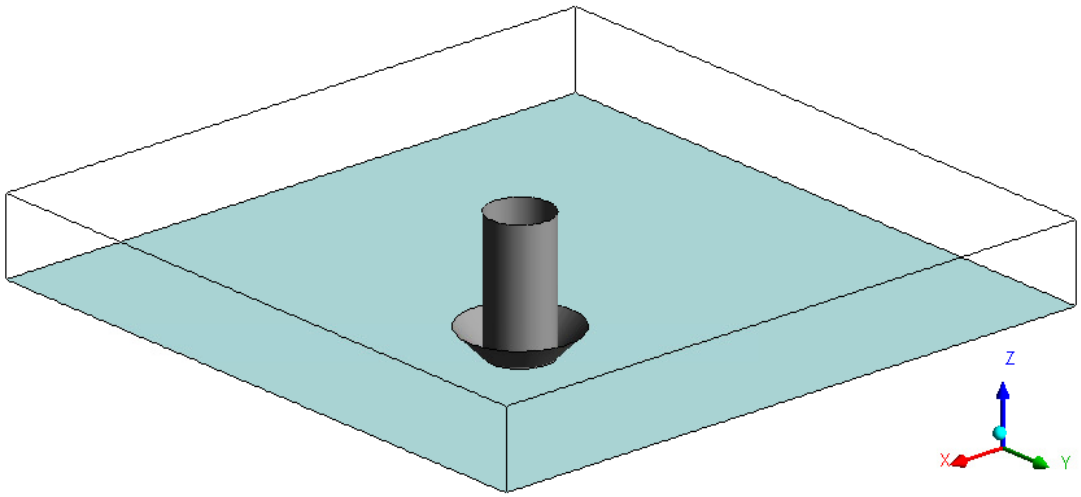

Figure 2: Geometry of the CFD model. The light turquoise and the dark grey surfaces represent the build platform and the extrusion nozzle, respectively.

Both immiscible phases were modeled as incompressible Newtonian fluids with constant material properties. The material parameters used in the numerical simulation are provided in Table 3. On the one hand, the molten polymer was assigned a density of 1.25 g/cm^3 and a viscosity of 1000 Pa·s. Although representative of actual polymer melts, these values do not affect the numerical results, as the material deposition is essentially a creeping flow. On the other hand, we did not wish to resolve the vortical flow of the air around the print head. Thus, the air phase was assigned artificial values of density (1.0×10^{-5} g/cm^3) and viscosity (0.01 Pa·s), in order to obtain a creeping flow in the air, thereby enhancing numerical convergence. The artificially large value of the air viscosity did not affect the free-surface of the molten polymer, as it was still 5 orders of magnitude lower than the polymer melt viscosity. Gravity was included in the model, but it did not affect the numerical results. Thermal shrinkage was neglected.

Table 3: Material parameters used in the numerical simulations.

Parameters	**Value**
Polymer melt density	1.25 g/cm^3
Polymer melt viscosity	1000 Pa·s
Air density	1.0×10^{-5} g/cm^3
Air viscosity	0.01 Pa·s
Standard gravity acceleration	-9.81 m/s^2

Results and discussions

The numerical simulations of the transient deposition flows provide predictions of the shape of the printed road at the 90° turn. The shape of the deposited roads is a result of the hydrodynamic forces. After extrusion, the deposition material is not subjected to deformation, and the shape of the road does not change anymore. The simulated shapes of the deposited roads are displayed in Figure 3, for the four deposition strategies investigated (see Table 2). Figure 4 shows close up views of the roads near the turn. We can see that the ideally synchronized extrusion rate and the

stop-at-turn trajectory (Case 1) produces a sharp corner with a uniform road width. Only a minimal amount of overfill and underfill are obtained at the interior and the exterior of the turn, because of the corner geometry. In contrast, the material deposition along the same stop-at-turn trajectory but with a constant extrusion rate (Case 2) yields a large overfill, due to the extra material deposited during the deceleration/acceleration phases, before and after the turn point. The extra deposited material is pushed on the side of the road, resulting in overfills on both the interior and exterior sides of the turn. In the third and fourth investigated deposition strategies, the extrusion rate is kept constant, but the printing head negotiates the turn with blended acceleration. The blended motion of the X and Y axis smooths the tool path trajectory and enable the possibility of printing the corner without stopping the printing head. In this way, the printing head is only subjected to a brief decrease of 30% and 50% of its cruising speed, for $\kappa = 1$ (Case 3) and $\kappa = 0.6$ (Case 4), respectively. The case $\kappa = 1$ results in slight variations of the road width along the turn, which comes at the expense of having a smoothed corner, as it can be seen in Figure 4. In the case where $\kappa = 0.6$, the road width undergoes larger variations than for $\kappa = 1$, but the extra deposited material compensates for the smoothed tool path, as it fills the exterior of the turn. Thus, Case 4 is a compromise between Case 2 and Case 3.

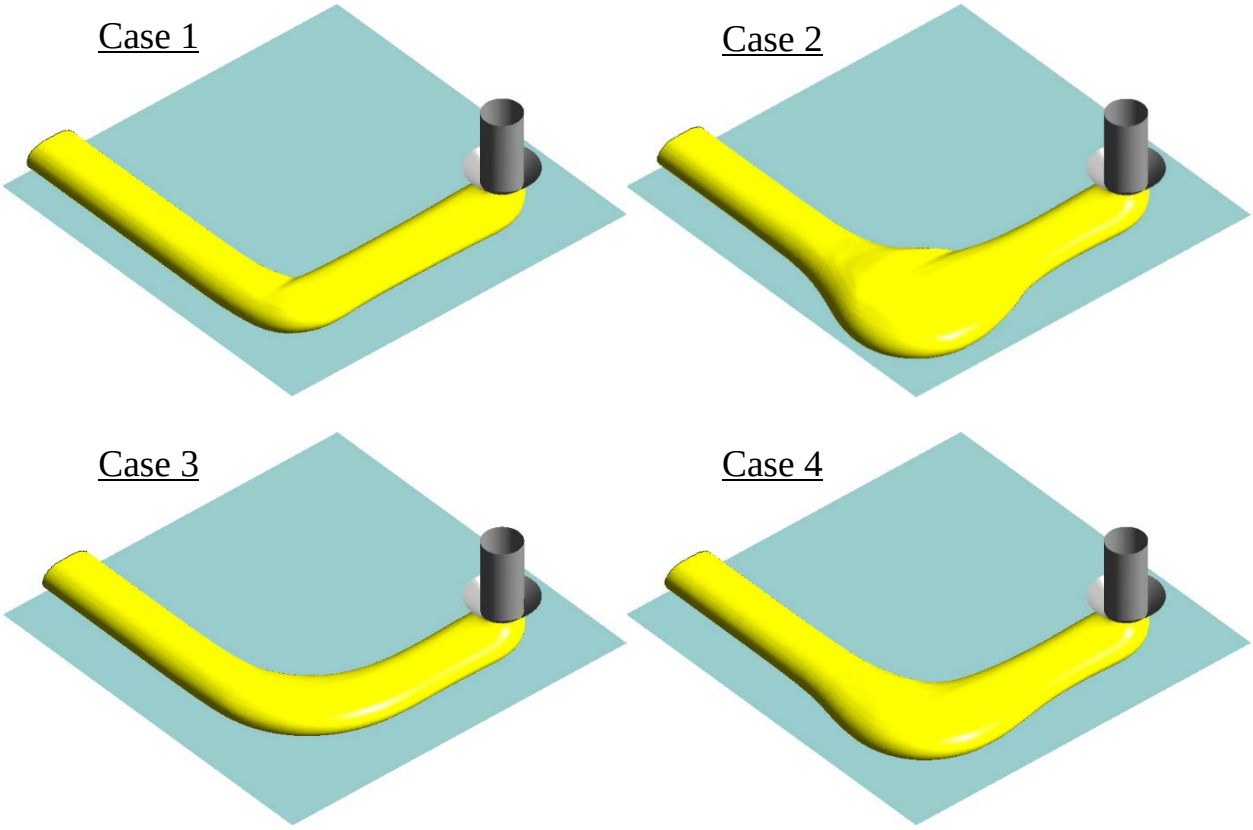

Figure 3: Simulations of the deposited road along a tool path with a 90° turn, for different deposition strategies (perspective views).

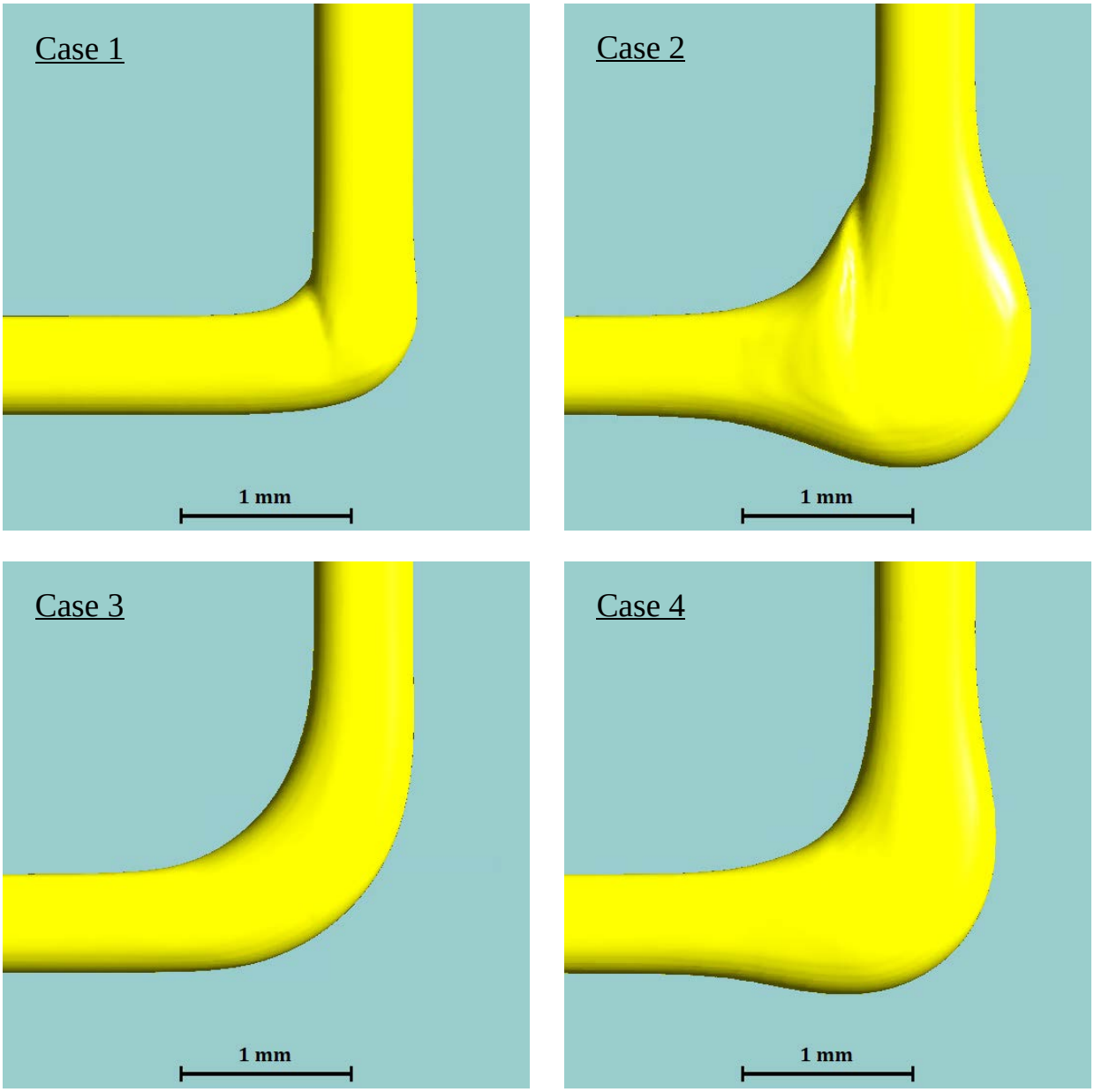

Figure 4: Close up views of the road near the turn, for different deposition strategies (top views).

Conclusion

We have used a CFD model to simulate material deposition in fused deposition modeling. The molten thermoplastic was modeled as a free-surface incompressible Newtonian fluid. The model has been used to predict the shape of a road printed onto the build platform, along a tool path with a 90° turn. Four deposition strategies have been investigated. The ideal case where the extrusion rate is synchronized with the tangential velocity of the printing head and the tool path follows a stop-at-turn trajectory produces a uniform road width with minimal overfill and underfill at the turn. Nonetheless, if the extrusion rate is kept constant during the acceleration and deceleration phases, the stop-at-turn trajectory yields a large overfill at the turn. An almost uniform road width can be obtained with a constant extrusion rate, by using blended acceleration, at the

expense of smoothing the corner. The smoothed tool path with an acceleration blending factor κ = 0.6 provides a compromise between material overfill and corner smoothing. In principle, the predicted variations of the road width at the corner could be taken into account by the tool path planner, in order to compensate overfill and underfill regions. Thus, CFD simulations could be used to develop optimized tool paths and deposition strategies, which would improve dimensional accuracy and surface quality in extrusion-based additive manufacturing.

Acknowledgments

The authors would like to acknowledge the support of the Danish Council for Independent Research (DFF) | Technology and Production Sciences (FTP) (Contract No. 7017-00128).

References

[1] B. N. Turner, R. Strong, S. A. Gold, A review of melt extrusion additive manufacturing processes: I. Process design and modeling, Rapid Prototyping Journal 20, 192-204 (2014).

[2] P. Kulkarni, D. Dutta, Deposition strategies and resulting part stiffnesses in fused deposition modeling, Journal of Manufacturing Science and Engineering 121, 93-103 (1999).

[3] B. N. Turner, S. A. Gold, A review of melt extrusion additive manufacturing processes: II. Materials, dimensional accuracy, and surface roughness, Rapid Prototyping Journal 21, 250-261 (2015).

[4] O. A. Mohamed, S. H. Masood, J. L. Bhowmik, Optimization of fused deposition modeling process parameters: a review of current research and future prospects, Advances in Manufacturing 3, 42-53 (2015).

[5] L. Santana, J. L. Alves, A. C. S. Netto, A study of parametric calibration for low cost 3D printing: Seeking improvement in dimensional quality, Materials & Design 135, 159-172 (2017).

[6] A. Jennings, 3D Printing Troubleshooting: 34 Common 3D Printing Problems, All3DP.com (2018), viewed on Apr. 1 2018. <https://all3dp.com/1/common-3d-printing-problems-troubleshooting-3d-printer-issues>

[7] Marlin [Computer software] (2018). <http://marlinfw.org>

[8] B. Weiss, D. W. Storti, M. A. Ganter, Low-cost closed-loop control of a 3D printer gantry, Rapid Prototyping Journal 21, 482-490 (2015).

[9] R. Comminal, M. P. Serdeczny, D. B. Pedersen, J. Spangenberg, Numerical modeling of the strand deposition flow in extrusion-based additive manufacturing, Additive Manufacturing 20, 68-76 (2018).

[10] J. Go, S. N. Schiffres, A. G. Stevens, A. J. Hart, Rate limits of additive manufacturing by fused filament fabrication and guidelines for high-throughput system design, Additive Manufacturing 16, 1-11 (2017).

[11] W. Han, M. A. Jafari, S. C. Danforth, A. Safari, Tool path-based deposition planning in fused deposition processes, Journal of Manufacturing Science and Engineering 124, 462-472 (2002).

[12] W. Han, M. A. Jafari, K. Seyed, Process speeding up via deposition planning in fused deposition-based layered manufacturing processes, Rapid Prototyping Journal 9, 212-218 (2003).

[13] A. Bouhal, M. A. Jafari, W. Han, T. Fang, Tracking control and trajectory planning in layered manufacturing applications, IEEE Transactions on Industrial Electronics 46, 445-451 (1999).

[14] W. Han, M. A. Jafari, Coordination control of positioning and deposition in layered manufacturing, IEEE Transactions on Industrial Electronics 54, 651-659 (2007).

[15] D. S. Ertay, A. Yuen, Y. Altintas, Synchronized material deposition rate control with path velocity on fused filament fabrication machines, Additive Manufacturing 19, 205-213 (2018).

[16] A. Bellini, S. Guceri, M. Bertoldi, Liquefier dynamics in fused deposition, Journal of Manufacturing Science and Engineering 126, 237-246 (2004).

[17] K. Y. Jiang, Y. H. Gu, Controlling parameters for polymer melting and extrusion in FDM, Key Engineering Materials 259, 667-671 (2004).

[18] M. E. Mackay, Z. R. Swain, C. R. Banbury, D. D. Phan, D. A. Edwards, The performance of the hot end in a plasticating 3D printer, Journal of Rheology 61, 229-236 (2017).

[19] J. Du, Z. Wei, X. Wang, J. Wang, Z. Chen, An improved fused deposition modeling process for forming large-size thin-walled parts, Journal of Materials Processing Technology 234, 332-341 (2016).

[20] H. Xia, J. Lu, S. Dabiri, G. Tryggvason, Fully resolved numerical simulations of fused deposition modeling. Part I: fluid flow, Rapid Prototyping Journal 24, 463-476 (2018).

[21] H. Xia, J. Lu, G. Tryggvason, Fully Resolved Numerical Simulations of Fused Deposition Modeling. Part II-Solidification, Residual Stresses, and Modeling of the Nozzle, arXiv preprint arXiv:1711.07094 (2017).

[22] ANSYS® FLUENT R18.2, ANSYS FLUENT Theory Guide, © ANSYS, Inc., (2017).